arXiv:1301.1189v1 [cond-mat.supr-con] 7 Jan 2013

Optimizing the spin sensitivity of grain boundary junction nanoSQUIDs – towards detection of small spin systems with single-spin resolution

R. Wölbing,[1] T. Schwarz,[1] J. Nagel,[1] M. Kemmler,[1] D. Koelle,[1] and R. Kleiner[1]

[1] *Physikalisches Institut – Experimentalphysik II and Center for Collective Quantum Phenomena in LISA$^+$,*
Universität Tübingen, Auf der Morgenstelle 14, D-72076 Tübingen, Germany

We present an optimization study for improving the spin sensitivity of nanoSQUIDs based on resistively shunted grain boundary Josephson junctions. In addition the dc SQUIDs contain a narrow constriction onto which a small magnetic particle can be placed with efficient coupling of its stray magnetic field to the SQUID loop. The separation of the location of optimum coupling from the junctions allows for an independent optimization of coupling and junction properties. Our analysis of the dependence of the flux noise of the SQUID and of the coupling of a magnetic particle on the geometric parameters of the SQUID layout shows that a spin sensitivity $S_\mu^{1/2}$ of a few $\mu_B/\sqrt{\mathrm{Hz}}$ should be feasible for optimized parameters, respecting technological constraints.

PACS numbers: 85.25.CP, 85.25.Dq, 74.78.Na, 74.72.-h 74.25.F- 74.40.De

I. INTRODUCTION

Miniaturized direct current (dc) superconducting quantum interference devices (SQUIDs) with dimensions in the sub-micrometer range (nanoSQUIDs) are promising devices for the sensitive detection and investigation of small spin systems.[1] The basic idea behind this is to attach a small (nanometer-sized) magnetic particle directly to the SQUID and trace out magnetic hysteresis loops of the particle. This shall be done by detecting the change of the stray magnetic field of the particle with magnetic moment $\vec{\mu}$ via the change of the magnetic flux Φ coupled to the SQUID loop.[2–4]. In order to meet the ultimate goal of detecting the flipping of only a few electron spins,[5] the spin sensitivity $S_\mu^{1/2} = S_\Phi^{1/2}/\phi_\mu$ has to be optimized carefully via reducing the spectral density of flux noise S_Φ of the SQUID and increasing the coupling factor $\phi_\mu \equiv \Phi/\mu$ (with $\mu \equiv |\vec{\mu}|$). S_Φ can be reduced by shrinking the size of the SQUID loop, and hence its inductance L, and ϕ_μ can be increased by placing the particle on a narrow constriction inserted in the SQUID loop, which motivates the need to implement sub-micron SQUID structures.

Until now, the most common approach for the realization of nanoSQUIDs is to use constriction type Josephson junctions intersecting small SQUID loops (see e.g. Ref. [6] published in a special issue on nanoSQUIDs and related articles therein). However, this approach comes with several drawbacks: Constriction type Josephson junctions often show hysteretic current-voltage characteristics (IVCs). This does not allow to operate the SQUID magnetometers continuously, which is required for the investigation of the magnetization dynamics of the sample under investigation. Furthermore, this does not allow to use advanced SQUID read-out electronics, which have been developed for SQUIDs with non-hysteretic Josephson junctions and which are required for the read-out of ultra-sensitive dc SQUIDs. Also, the noise properties of such junctions are not well understood and hence hard to optimize. And, finally, the magnetic particles have to be placed close to the constriction type junctions in order to achieve optimum coupling. However, this means that the junction properties and the coupling factor ϕ_μ cannot be optimized independently, which hampers a careful optimization of the spin sensitivity.

We should note here, that very sensitive Nb thin film nanoSQUIDs based on constriction type junctions, resistively shunted with a thin W layer, have been realized.[7] However, in this case, the devices show optimum performance only in a narrow range of temperature T not too far below the transition temperature T_c of Nb, which makes them less interesting for applications. With respect to the application of nanoSQUIDs for the detection of the magnetization reversal of nanomagnets, the most interesting regime of operation is at $T \approx 1\,\mathrm{K}$ and below and at very high magnetic fields in the tesla range.[1] It has been demonstrated that Nb thin film nanoSQUIDs based on constriction type junctions can be operated in impressive background fields up to $7\,\mathrm{T}$.[8] However, the upper critical field of typical Nb thin films ($\sim 1\,\mathrm{T}$) requires to use very thin Nb films with thicknesses of only a few nm, i.e. well below the London penetration depth λ_L of the Nb films, if such SQUIDs shall be operated in tesla fields. This leads to a large kinetic inductance contribution to the SQUID inductance, and hence a large flux noise of such SQUIDs, which does not allow to use the huge potential for the realization of ultralow-noise nanoSQUIDs.

In order to circumvent the above mentioned drawbacks, we recently started to develop dc nanoSQUIDs based on $\mathrm{YBa_2Cu_3O_7}$ (YBCO) thin films with submicron wide bicrystal grain boundary Josephson junctions (GBJs).[9] Due to the huge upper critical field of YBCO, such SQUIDs can be realized with film thicknesses on the order of λ_L and above and operated in tesla fields. Furthermore, due to the large critical current densities of the YBCO GBJs (several $10^5\,\mathrm{A/cm^2}$ at $T = 4.2\,\mathrm{K}$ and below for a grain boundary misorientation angle of 24°) submicron junctions still yield reasonably large values of the critical current I_0. In order to achieve non-hysteretic

IVCs, the GBJs are shunted by a thin Au film. Due to the fact that the barrier of the GBJs is oriented perpendicular to the YBCO thin film plane, it is possible to apply tesla magnetic fields in the plane of the film, without a significant reduction of I_0.[10] And finally, implementing an additional narrow constriction (which can be much narrower than the GBJs) in the SQUID loop, the optimization of the coupling factor is possible without affecting the junction properties.

Here, we present a detailed optimization study of the spin sensitivity of such grain boundary junction nanoSQUIDs by analyzing the dependence of the flux noise S_Φ and the coupling factor ϕ_μ on the geometry of our devices. We find that for an optimized SQUID geometry a continuous detection of magnetic moments down to a spin sensitivity $S_\mu^{1/2}$ of a few $\mu_B/\sqrt{\mathrm{Hz}}$ is feasible (μ_B is the Bohr magneton).

II. NANOSQUID DESIGN

The layout of the nanoSQUID (top view) is shown in Fig. 1. The SQUID structure is patterned in a YBCO thin film of thickness d, covered by a thin Au film with thickness d_{Au}. The two bridges straddling the grain boundary have a width w_J and length l_J. The upper part of the SQUID loop contains a constriction of width w_c and length l_c. An applied bias current I is flowing from top to bottom across the two GBJs. A small magnetic particle can be placed on top of the constriction, and an in-plane magnetic field (perpendicular to the grain boundary) can be applied without significant suppression of the critical current I_0 of the two GBJs.

Optimizing the SQUID for spin sensitivity means to minimize the ratio S_Φ/ϕ_μ^2. The coupling factor ϕ_μ is essentially determined by the geometry of the constriction, i.e., its width w_c and thickness d. S_Φ depends on the SQUID inductance L and on the junction parameters I_0, resistance R and capacitance C. If the constriction could be made not only arbitrarily thin and narrow, but also arbitrarily short, one could envision a scenario, where ϕ_μ reaches a value around $0.5\,\Phi_0/\mu_B$,[4] while, at the same time, the inductance of the constriction remains small (Φ_0 is the magnetic flux quantum). Then, S_Φ could be optimized independently by proper choice of the SQUID size and the junction properties. For the type of device we discuss here, this is certainly not the case and we thus look for an optimization, which is compatible with technological limitations. A large coupling ϕ_μ demands as narrow and thin as possible constrictions. On the other hand, for too narrow constrictions, given a fixed value of d, its inductance L_c and thus also the total inductance L of the SQUID may become too large, possibly degrading the flux noise. This may be counterbalanced by choosing a different film thickness and changing, e.g., the junction width w_J.

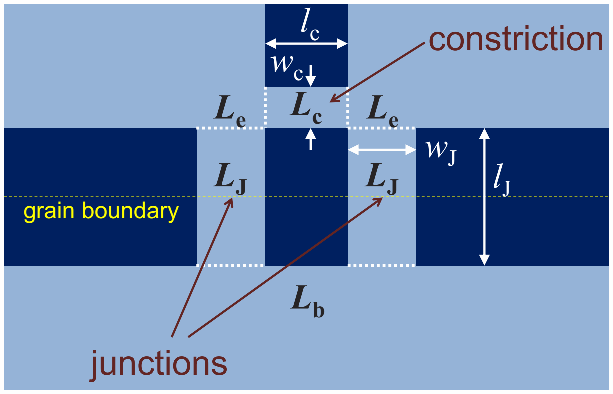

FIG. 1: (Color online) Schematic view of the nanoSQUID layout, divided (by white dotted lines) into the constriction (inductance L_c, length l_c, width w_c), two corners (each with inductance L_e), the two junctions (each with inductance L_J, length l_J, width w_J) and the bottom part (inductance L_b).

In the following sections, we derive explicit expressions for the dependence of ϕ_μ (Sec. III) and S_Φ (Sec. IV) on various geometric and electric SQUID parameters, which then allows us to optimize S_μ (Sec. V).

III. COUPLING FACTOR

We numerically calculate the coupling factor $\phi_\mu = \Phi/\mu$, i.e. the flux Φ coupled into the SQUID loop by a point-like particle with magnetic moment μ, using the software package 3D-MLSI, which solves the London equations.[11] Details on the calculation procedure can be found in Ref. [9]. In brief, for a given SQUID geometry (cf. Fig. 1), one calculates the magnetic field distribution $\vec{B}(\vec{r})$ generated by a current J circulating around the SQUID hole. The coupling factor is obtained from $\phi_\mu = -\widehat{e}_\mu \vec{B}(\vec{r})/J$. Here, $\widehat{e}_\mu$ is the direction of the magnetic moment $\vec{\mu}$ at position $\vec{r}$.

For a particle with its magnetic moment oriented in the plane of the thin film SQUID perpendicular to the grain boundary, we find a maximum ϕ_μ if the particle is placed directly on top of and as close as possible to the constriction.[10] Assuming that a particle is placed at a distance of 10 nm above the constriction (without an Au layer, which can be removed without affecting the junction properties), we calculate ϕ_μ in the range $40\,\mathrm{nm} < w_c < 200\,\mathrm{nm}$ and $40\,\mathrm{nm} < d < 500\,\mathrm{nm}$ and find the dependence

$$\phi_\mu \approx \gamma_\mu \left(\frac{w_0}{w_c}\right)^{0.7} (12.3 + \frac{d_0}{d}) \,, \qquad (1)$$

with $d_0 = 320\,\mathrm{nm}$, $w_0 = 1\,\mathrm{nm}$ and $\gamma_\mu = 23\,\mathrm{n}\Phi_0/\mu_B$.

As expected, we find a decreasing ϕ_μ with increasing width w_c of the constriction. Our simulations yield $\phi_\mu \propto w_c^{-0.7}$, i.e., a change in ϕ_μ by a factor of 3 within the simulation range used for w_c. Furthermore, ϕ_μ also decreases with increasing film thickness d. However, within the (larger) simulation range for d, we find a much weaker dependence on d; in particular, for $d \gtrsim d_0$, the coupling starts to saturate. We note that some uncertainty in determining ϕ_μ arises from the fact, that 3D-MLSI uses supercurrents that flow only within a 2D layer. Hence, in the constriction region – in particular in the case of a large aspect ratio d/w_c – there may be a nontrivial 3D current flow. As a consequence, the prediction of a saturation of ϕ_μ with increasing d may not be correct. On the other hand, we will show below, that S_Φ shows clearly a stronger dependence on d than ϕ_μ does. Hence, for the optimization of S_μ the uncertainty in $\phi_\mu(d)$ is not very critical.

IV. FLUX NOISE

In order to determine the flux noise of the SQUID, we use the theoretical expression obtained from Langevin simulations,

$$S_\Phi = f(\beta_L)\Phi_0 k_B T L / I_0 R, \tag{2}$$

which is valid for a Stewart-McCumber parameter $\beta_C \equiv 2\pi I_0 R^2 C/\Phi_0 \lesssim 1$ and $\Gamma\beta_L < 0.1$.[12] Here, $\Gamma \equiv 2\pi k_B T/I_0\Phi_0$ is the noise parameter, and $\beta_L \equiv 2LI_0/\Phi_0$ is the screening parameter. For $\beta_L > 0.4$, $f(\beta_L) \approx 4(1+\beta_L)$. For lower values of β_L, S_Φ increases.

The first factor to be discussed is I_0R. The junction resistance R can be varied to some extent by varying the thickness $d_{\rm Au}$ of the Au layer covering the YBCO film; the maximum achievable value is the unshunted junction normal state resistance R_N (for $d_{\rm Au} = 0$). For 24° YBCO grain boundary junctions, I_0R_N values $\sim 2-3\,$mV are achievable at $4.2\,$K.[13] However, such junctions typically have hysteretic IVCs. We thus demand $\beta_C \lesssim 1$ to avoid hysteresis. Ideally, one would like to derive an expression for I_0R as a function of w_J, d and $d_{\rm Au}$ using the constraint $\beta_C \lesssim 1$ and assuming certain values for the critical current density j_0, unshunted normal junction resistance times area $\rho \equiv R_N w_J d$ and capacitance per junction area C'. However, the scaling of R with w_J, d and $d_{\rm Au}$ is currently not known. Furthermore, an estimate of C' as a function of w_J and d, based on various scaling laws available in the literature,[14–16], is quite difficult, in particular since it is difficult to determine C for underdamped YBCO GBJs and since the stray capacitance due to the commonly used SrTiO$_3$ substrates may play an important role.[17] On the other hand, we have fabricated 24° YBCO GBJs with different junction width and film thickness ($w_J = 450\,$nm, $d = 50\,$nm and $w_J = 330\,$nm, $d = 300\,$nm), using the focused ion beam (FIB) milling technique as described in[10]. Those junctions had only weakly hysteretic IVCs but $I_0R \approx 1\,$mV at $T = 4.2\,$K. Below we will find an optimum junction width $w_J \sim 260\,$nm (for $d = 300\,$nm), which is not much below the width of those junctions. Thus, rather than introducing an ill-defined scaling of I_0R with w_J and d, below we fix I_0R and use $1\,$mV as a realistic value.

We next determine the dependence of the SQUID inductance L on the various geometrical parameters. We separate the SQUID into the constriction (inductance L_c, length l_c, width w_c), the two (symmetric) bridges containing the junctions (inductance L_J, length l_J, width w_J), the two corners connecting the constriction and the junction arms (inductance L_e), and the bottom part of the SQUID (inductance L_b), as indicated in Fig. 1. Then, L is given by

$$L = L_c + 2L_J + 2L_e + L_b\ , \tag{3}$$

We should find $L_c(w_c, l_c, d)$, $L_J(w_J, l_J, d)$, $L_e(w_c, w_J, d)$ and $L_b(l_c, w_J, d)$. Trivially, l_c and l_J should be as small as possible. From simulations, using 3D-MLSI with $\lambda_L = 335\,$nm,[19] we find the parametrization $L_c(w_c, l_c, d) \approx L' \cdot l_c/(w_c d)$, where $L' = 143\,$pH·nm. This expression fits the simulated L_c well, within the parameter range $40\,{\rm nm} < w_c < 300\,{\rm nm}$ and $40\,{\rm nm} < d < 500\,{\rm nm}$, covered by the simulations. We use the same parametrization for $L_J(w_J, l_J, d)$. For the corners we find, within a 15 % variation with respect to w_J and w_c, the expression $L_e \approx L'_e/d$, with $L'_e = 100\,$pH·nm. Finally, we find $L_b \approx L'_b l_c/w_J d + L''_b/d$, with $L'_b = 45\,$pH·nm and $L''_b = 150\,$pH·nm. Inserting these expressions into Eq. (3) yields

$$L \approx \frac{L'}{d}\left\{\frac{l_c}{w_c} + \frac{(2l_j + bl_c)}{w_J} + r\right\}, \tag{4}$$

with $b \equiv L'_b/L' = 0.315$ and $r \equiv (2L'_e + L''_b)/L' = 2.45$.

For the minimization of S_μ, we will use β_L as a variable parameter. Since both, L and w_J are not independent of each other and are related to β_L, we express both as functions of β_L. This will allow us to eliminate L and w_J in the final expression for S_μ which has to be optimized. With $\beta_L = 2I_0L/\Phi_0$ and $I_0 = j_0 w_J d$, we obtain $w_J(\beta_L, L) = \Phi_0\beta_L/2j_0 dL$. Inserting this into Eq. (4) yields

$$L(\beta_L) \approx \frac{L'}{d}\left(\frac{l_c}{w_c} + r\right)\left\{1 - \frac{\kappa}{\beta_L}\right\}^{-1} \tag{5}$$

with $\kappa(l_J, l_c, j_0) \equiv 2(2l_J + bl_c)j_0L'/\Phi_0$.

Inserting Eq. (5) into Eq. (2) and using $f(\beta_L) = 4(1+\beta_L)$ finally yields

$$S_\Phi \approx S_{\Phi,0}\frac{d_0}{d}\left(\frac{l_c}{w_c} + r\right)\frac{1+\beta_L}{1-\frac{\kappa}{\beta_L}} \tag{6}$$

with $S^{1/2}_{\Phi,0} \equiv 2\sqrt{\frac{\Phi_0 k_B T L'}{I_0 R d_0}} = 7.1\,{\rm n}\Phi_0/\sqrt{\rm Hz}$ at $T = 4.2\,$K and with $I_0R = 1\,$mV. The most important result here is the scaling $S_\Phi \propto 1/d$. This is due to the fact that the SQUID inductance $L \propto 1/d$ within the simulation range for d because of the increase of the kinetic inductance contribution with decreasing d below λ_L. For $d \gtrsim 2\lambda_L$ we expect a saturation of $L(d)$ and hence of $S_\Phi(d)$. However, we will neglect this for the optimization of S_μ, since values for $d \gtrsim 500\,$nm are outside the simulation range for $L(d)$ and since we cannot expected to produce high-quality GBJs for such large values of d.

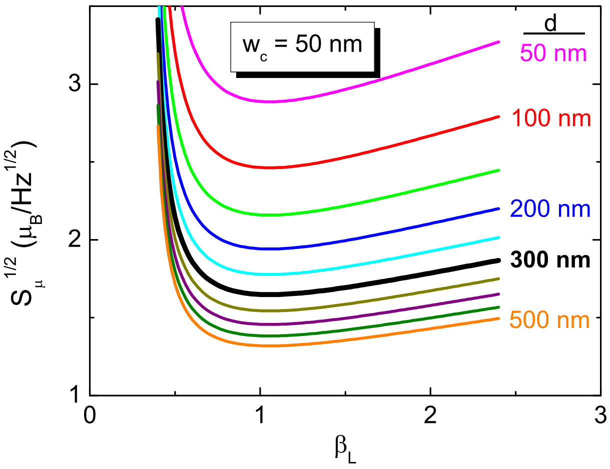

FIG. 2: (Color online) Spin sensitivity $S_\mu^{1/2}(\beta_L)$, calculated from Eq. (7) at $T = 4.2\,\mathrm{K}$ for 10 values of film thickness d (in 50 nm steps), with constriction width $w_c = 50\,\mathrm{nm}$ (and $l_c = 200\,\mathrm{nm}$, $l_J = 400\,\mathrm{nm}$, $j_0 = 3\,\mathrm{mA}/\mu\mathrm{m}^2$).

V. OPTIMIZATION OF SPIN SENSITIVITY VIA IMPROVED SQUID GEOMETRY

With Eq. (1) and (6) we can express the spin sensitivity as

$$S_\mu^{1/2} \approx S_{\mu,0}^{1/2}\,\frac{\sqrt{\frac{d}{d_0}}}{12.3\frac{d}{d_0}+1}\left(\frac{w_c}{w_0}\right)^{0.7}\sqrt{\frac{l_c}{w_c}+r}\,\sqrt{\frac{1+\beta_L}{1-\frac{\kappa}{\beta_L}}} \tag{7}$$

with $S_{\mu,0}^{1/2} \equiv S_{\Phi,0}^{1/2}/\gamma_\mu = 0.31\mu_B/\sqrt{\mathrm{Hz}}$ at $T = 4.2\,\mathrm{K}$ and with $I_0R = 1\,\mathrm{mV}$.

The evaluation of Eq. (7) shows that the minimization of $S_\mu^{1/2}(\beta_L, d, w_c, l_c, l_J)$ requires to make l_c and l_J as small as possible. Due to technological limitations, we use $l_c = 200\,\mathrm{nm}$ and $l_J = 400\,\mathrm{nm}$ below. The constriction width enters Eq. (7) via the factors $w_c^{0.7}(l_c/w_c + r)^{1/2}$, demanding w_c to be made as small as possible. Furthermore, $S_\mu^{1/2}$ decreases with increasing d within the simulation range; for large enough values of d, we find $S_\mu^{1/2} \propto 1/\sqrt{d}$. Hence, the film thickness should be as large as possible, respecting technological constraints. As mentioned at the end of Sec. IV, we expect L and hence S_Φ to saturate for $d \gtrsim 2\lambda_L$. In this case, which lies outside our simulation range, we expect $S_\mu^{1/2}$ to increase again with increasing d, due to the degradation of ϕ_μ. Hence, we should expect a minimum in $S_\mu^{1/2}$ for an optimum d, which however lies above our simulation range and also above technologically feasible values for d.

The dependence $S_\mu^{1/2}(\beta_L)$ at $T = 4.2\,\mathrm{K}$ is shown in Fig. 2 for various values of d, with fixed $w_c = 50\,\mathrm{nm}$. All curves exhibit a shallow minimum at a value which can be calculated from Eq. (7) as $\beta_{L,min} = \kappa(1+\sqrt{1+\kappa^{-1}})$. With the (fixed) values for l_c and l_J and with $j_0 = 3\,\mathrm{mA}/\mu\mathrm{m}^2$, we obtain $\kappa = 0.36$ and $\beta_{L,min} = 1.05$. For a reasonable value $d = 300\,\mathrm{nm}$ (cf. thick line in Fig. 2) we obtain $S_\Phi^{1/2} \approx 33\,\mathrm{n}\Phi_0/\sqrt{\mathrm{Hz}}$, $\phi_\mu = 20\,\mathrm{n}\Phi_0/\mu_B$ and $S_\mu^{1/2} \approx 1.6\,\mu_B/\sqrt{\mathrm{Hz}}$. Corresponding SQUID parameters are listed in Table I ("opt. device 1").

This is a drastic improvement, compared to the experimental value $S_\mu^{1/2} \approx 60\,\mu_B/\sqrt{\mathrm{Hz}}$ for our, so far, best experimental device with parameters $d = 60\,\mathrm{nm}$, $w_c = 90\,\mathrm{nm}$, $w_J = 130\,\mathrm{nm}$, $\beta_L = 0.65$, $L = 36\,\mathrm{pH}$, $I_0R = 0.13\,\mathrm{mV}$, $S_\Phi^{1/2} = 1.3\,\mu\Phi_0/\sqrt{\mathrm{Hz}}$ and $\phi_\mu = 21\,\mathrm{n}\Phi_0/\mu_B$.[10] The main improvement of $S_\mu^{1/2}$ comes from $S_\Phi^{1/2}$. Before discussing the various factors improving this quantity, we should say, however, that standard YBCO SQUIDs often have a $S_\Phi^{1/2}$, which is a factor of 2–10 higher than the theoretical predictions[18] (for the experimental device mentioned above $S_\Phi^{1/2}$ was a factor ~ 6 higher than predicted by Eq. (2)). In this respect we expect the theoretical $S_\Phi^{1/2}$ to be by a factor $\sim$ 2–10 too low, even if all factors entering $S_\Phi^{1/2}$ are feasible.

One major improvement of $S_\Phi^{1/2}$ arises from the total SQUID inductance L, which is almost an order of magnitude lower than the inductance of our experimental device. This is mainly because of the much larger value of d. The low value of L seems realistic; in terms of geometrical factors, $w_c = 50\,\mathrm{nm}$ and lengths l_c and l_J are chosen sportive, but not impossible. This is supported by preliminary tests, which show that 300 nm thick YBCO films can be patterned properly by FIB milling.

Another big improvement of $S_\Phi^{1/2}$ comes from the optimized value of I_0R, which is by a factor of ~ 8 higher than that of our experimental device. For narrow ($w_J \sim 100\,\mathrm{nm}$) and thin ($d \sim 50\,\mathrm{nm}$) junctions this would be impossible to achieve.[9] However, the optimization yielded much wider ($w_J \sim 260\,\mathrm{nm}$) and thicker ($d \sim 300\,\mathrm{nm}$) junctions, for which we have already found that $I_0R \sim 1\,\mathrm{mV}$ is achievable.

Finally, we note that, if we take more easily achievable values $d = 200\,\mathrm{nm}$ and $w_c = 100\,\mathrm{nm}$ (other input parameters are the same as for the initial optimization), we still get $S_\mu^{1/2} = 2.6\,\mu_B/\sqrt{\mathrm{Hz}}$, with parameter values $w_J = 375\,\mathrm{nm}$, $L = 4.8\,\mathrm{pH}$, $I_0 = 225\,\mu\mathrm{A}$ and $R = 4.44\,\Omega$ (see Table. I for parameters of "opt. device 2"). The resulting $S_\mu^{1/2}$ is less than a factor of 2 different from the value obtained for the initial input parameters, so that we are optimistic that the design discussed in this paper is indeed capable of obtaining a spin sensitivity in the range of a few $\mu_B/\sqrt{\mathrm{Hz}}$.

VI. CONCLUSIONS

In summary, we have performed a detailed analysis of the coupling factor ϕ_μ and the spectral density of flux noise S_Φ, and hence of the spin sensitivity $S_\mu^{1/2} = S_\Phi^{1/2}/\phi_\mu$ of a grain boundary junction dc nanoSQUID. Based on the calculation of ϕ_μ and S_Φ, we derived an explicit expression for the spin sensitivity $S_\mu^{1/2}$ as a function

	d	l_c	l_j	w_c	w_J	β_L	L	I_0	R	I_0R	j_0	L_c	L_J	L_e	L_b	$S_\Phi^{1/2}$	ϕ_μ	$S_\mu^{1/2}$
units	nm	nm	nm	nm	nm		pH	μA	Ω	mV	mA/μm^2	pH	pH	pH	pH	n$\Phi_0/\sqrt{\text{Hz}}$	nΦ_0/μ_B	$\mu_B/\sqrt{\text{Hz}}$
opt. device1	300	200	400	50	260	1.05	4.7	233	4.30	1	3	1.9	0.74	0.33	0.62	32.7	19.9	1.65
opt. device2	200	200	400	100	375	1.05	4.8	225	4.44	1	3	1.4	0.76	0.50	0.87	33.3	12.7	2.62

TABLE I: Summary of geometric and electric nanoSQUID parameters (as defined in the text). The values for "opt. device 1" are calculated for an optimized device with film thickness $d = 300\,\text{nm}$ and constriction width $w_c = 50\,\text{nm}$. The values for "opt. device 2" are calculated for more relaxed values $d = 200\,\text{nm}$ and $w_c = 100\,\text{nm}$ and otherwise identical input parameters for l_c, l_J, I_0R and (optimum) β_L.

of the geometric and electrical parameters of our devices. This allows for an optimization of $S_\mu^{1/2}$, which predicts a spin sensitivity of a few $\mu_B/\sqrt{\text{Hz}}$. Such a low value for $S_\mu^{1/2}$ can be achieved by realization of very low inductance nanoSQUIDs with ultra-low flux noise on the order of only a few tens of n$\Phi_0/\sqrt{\text{Hz}}$. This poses severe challenges on proper readout electronics for such SQUIDs. It remains to be shown whether or not the readout of such ultralow-noise SQUIDs is feasible and whether or not the envisaged values for the spin sensitivity can also be achieved in high fields, which is a major driving force for using these grain boundary junction nanoSQUIDs.

Acknowledgments

J. Nagel and T. Schwarz acknowledge support by the Carl-Zeiss-Stiftung. This work was funded by the Nachwuchswissenschaftlerprogramm of the Universität Tübingen, by the Deutsche Forschungsgemeinschaft (DFG) via the SFB/TRR 21 and by the European Research Council via SOCATHES.

---

[1] W. Wernsdorfer, Adv. Chem. Phys. **118**, 99 (2001).

[2] M. Ketchen, D. Awschalom, W. Gallagher, A. Kleinsasser, R. Sandstrom, J. Rozen, and B. Bumble, IEEE Trans. Magn. **25**, 1212 (1989).

[3] W. Wernsdorfer, D. Mailly, and A. Benoit, J. Appl. Phys. **87**, 5094 (2000).

[4] V. Bouchiat, Supercond. Sci. Technol. **22**, 064002 (2009).

[5] J. Gallop, Supercond. Sci. Technol. **16**, 1575 (2003).

[6] C. P. Foley and H. Hilgenkamp, Supercond. Sci. Technol. **22**, 064001 (2009).

[7] L. Hao, J. C. Macfarlane, J. C. Gallop, D. Cox, J. Beyer, D. Drung, and T. Schurig, Appl. Phys. Lett. **92**, 192507 (2008).

[8] L. Chen, W. Wernsdorfer, C. Lampropoulos, G. Christou, and I. Chiorescu, Nanotechnol. **21**, 405504 (2010).

[9] J. Nagel, K. B. Konovalenko, M. Kemmler, M. Turad, R. Werner, E. Kleisz, S. Menzel, R. Klingeler, B. Büchner, R. Kleiner, et al., Supercond. Sci. Technol. **24**, 015015 (2011).

[10] T. Schwarz, J. Nagel, R. Wölbing, M. Kemmler, R. Kleiner, and D. Koelle, ACS Nano (2012), in press; DOI: 10.1021/nn305431c.

[11] M. Khapaev, M. Kupriyanov, E. Goldobin, and M. Siegel, Supercond. Sci. Technol. **16**, 24 (2003).

[12] B. Chesca, R. Kleiner, and D. Koelle, in The SQUD Handbook, edited by J. Clarke and A. I. Braginski (Wiley-VCH, Weinheim, 2004), vol. 1: Fundamentals and Technology of SQUIDs and SQUID systems, chap. 2, pp. 29–92.

[13] H. Hilgenkamp and J. Mannhart, Rev. Mod. Phys. **74**, 485 (2002).

[14] B. H. Moeckly and R. A. Buhrman, IEEE Trans. Appl. Supecond. **5**, 3414 (2005).

[15] P. F. McBrien, R. H. Hadfield, W. E. Booij, A. Moya, F. Kahlmann, M. G. Blamire, C. M. Pegrum, and E. J. Tarte, Physica C **339**, 88 (2000).

[16] M. A. Navacerrada, M. L. Lucía, L. L. Sánchez-Soto, F. Sánchez Quesada, E. Sarnelli, and G. Testa, Phys. Rev. B **71**, 014501 (2005).

[17] A. Beck, O. Froehlich, D. Koelle, R. Gross, H. Sato, and M. Naito, Appl. Phys. Lett. **68**, 3341 (1996).

[18] D. Koelle, R. Kleiner, F. Ludwig, E. Dantsker, and J. Clarke, Rev. Mod. Phys. **71**, 631 (1999).

[19] For YBCO SQUIDs, 3D-MLSI is known to predict too low inductances if a proper value for λ_L ($\approx 180\,\text{nm}$) is used. The reason is unclear but may have to do with the layered structure and anisotropy of YBCO. In our simulations we have increased λ_L to be consistent with the experimentally determined values of L